42nd AIAA/ASME/SAE/ASEE Joint Propulsion Conference & Exhibit
9 - 12 July 2006, Sacramento, California

AIAA 2006-5173

Mobility Studies of a Pure Electron Plasma in Hall Thruster Fields

Emily C. Fossum,* Lyon B. King,† and Jason Makela‡
Michigan Technological University, Houghton, MI, 49931, U.S.A

An electron trapping apparatus was constructed in order to study electron dynamics in the defining electric and magnetic fields of a Hall-effect thruster. The approach presented here decouples the cross-field mobility from plasma effects by conducting measurements on a pure electron plasma in a highly controlled environment. Dielectric walls are removed completely eliminating all wall effects; thus, electrons are confined solely by a radial magnetic field and a crossed, independently-controlled, axial electric field that induces the closed-drift azimuthal Hall current. Electron trajectories and cross-field mobility were examined in response to electric and magnetic field strength and background neutral density. Without wall effects or neutral plasma effects mobility is presumed to follow the classical mobility model. In the present research, measurement techniques are investigated, and results are verified against the classical model. Preliminary findings suggest that that the apparatus and techniques used will be valid for mobility studies in more complex field environments.

Nomenclature

A_a	=	anode surface area
A_p	=	probe surface area
B_r	=	radial magnetic field
$\mathbf{B}$	=	magnetic field vector
B	=	magnitude of $\mathbf{B}$
$\hat{b}$	=	unit vector in the **B**-field direction
ε_0	=	permittivity of free space
$\mathbf{E}$	=	electric field vector
E_z	=	axial electric field
I_d	=	mobility drift current
I_a	=	anode current
I_p	=	probe current
J_a	=	current density at the anode
$J_{e\theta}$	=	Hall current density
J_{ez}	=	cross-field electron current density,
J_p	=	current density at the probe
m_e	=	electron mass
μ, μ_0	=	magnetic moment of gyrating particle
μ_{ez}	=	cross-field electron mobility
n_e	=	electron number density
ν_{ne}	=	electron-neutral collision frequency
q	=	particle charge
r_{Le}	=	electron Larmor radius
r_{Li}	=	ion Larmor radius
u_{eB}	=	electron bounce velocity

* GRA, Mechanical Engineering, ecfossum@mtu.edu
† Associate Professor, Mechanical Engineering, lbking@mtu.edu
‡ GRA, Mechanical Engineering, jmakela@mtu.edu

$u_{e\theta}$ = azimuthal electron velocity
u_{ez} = cross-field electron velocity
v_e = electron perpendicular velocity
Φ = electric potential
Φ_{eff} = effective trap potential
ω_{ce} = electron cyclotron frequency
ω_B = bounce frequency
Ω = magnetron frequency
Ω_H = electron Hall parameter

I. Introduction

THE defining characteristic of Hall thrusters is the crossed axial electric and radial magnetic fields. The criteria of the E- and B-fields are such that the electron gyro radius is small compared with apparatus dimensions while the gyro radius and mean free path for ions are larger than apparatus dimensions; these criteria are necessary so that ions are only affected by the electric field, whereas the electron trajectories are controlled by both electric and magnetic fields. The purpose of the radial magnetic field in a Hall thruster is to impede electron flow toward the anode, which maintains the axial electric field necessary to accelerate large, unmagnetized propellant ions. The crossed E and B fields induce the confining **E**x**B** electron drift which holds electrons in azimuthal orbits around the discharge channel annulus. Electrons slowly diffuse across the radial B-field lines, gaining energy from the E-field and dissipating this energy through wall collisions and electron-neutral collisions, which ionize propellant neutrals. This cross-field electron transport is obviously necessary to sustain thruster discharge; however, mobility takes energy away from the accelerating region, which, in excess, has negative effect on thruster efficiency. In past experiments the cross-field electron mobility has been found to be much larger than the classical collisional diffusion model, which states that electrons cross field lines by electron-neutral collisions alone[1,2].

The anomalous electron mobility was first observed in Hall thruster fields by Janes and Lowder[1] and later supported by Meezan et al[2], who observed mobility up to 1,000 times greater than predicted by classical theory. Janes and Lowder predicted this departure to be caused in part by azimuthal fluctuations in plasma density, and thus electric field, creating a secondary drift term in the axial direction. Plasma fluctuations have since been characterized and are now well documented[3] leading to Meezen's work supporting Janes and Lowder's initial hypothesis. Meezen provided the first quantified measure of mobility as it varies with axial position in the discharge channel, finding the greatest departure from the classical model at the location where plasma fluctuations were shown to exist. Others have hypothesized that the dielectric wall interactions play a significant role in electron transport, and attempts have been made to quantify and model the near wall region of the discharge channel[4,5]. To support the significance of wall interactions, King[6], through a comprehensive study of forces in the discharge channel, described the necessity of a negative sheath on the outer dielectric wall in order to close the azimuthal ExB drift, expressing a radial E-field force ten times that of the magnetic mirror force acting on electrons at the outer wall. Without this negative sheath, which is responsible for the confining electric field, the dominant electron motion is toward the walls, resulting in multiple wall collisions in a single azimuthal orbit and a net current to the walls until this negative sheath is formed and sustained.

The approach used in this investigation removes such plasma fluctuations and wall interactions by examining the electron dynamics of a pure electron plasma in a Hall thruster's defining fields with an independently-controlled electric field in vacuum. Mobility studies were performed in a highly controlled environment disconnected from the coupling ion and neutral plasma effects that usually control *and* are controlled by the field environment. Also absent were the dielectric walls and consequently the sheath that exists adjacent to the dielectric surface. The properties of the sheath and pre-sheath region are complex and not easily defined. Removing these complexities allows the electric field to be known at all points within the apparatus allowing for greatly simplified diagnostics. While such an approach has not been documented in Hall thruster studies, an examination of non-neutral plasma has proven to be useful for numerous types of charged particle transport studies,[7,8] examples being the Electron Diffusion Gauge (EDG) experiments of Chao and Davidson,[9] the measurement of neo-classic mobility by Robertson,[10,11,12] and numerous other related work involving positrons and ions.[13] Without plasma fluctuations or wall-interactions, mobility in such Hall thruster fields can be studied in its purest sense and a comparison with classical and experimental mobility can be made.

II. Mobility Concepts

In a Hall thruster the magnitude of the B-field is adjusted such that the electron Larmor radius is much less than the thruster size, while the ion Larmor radius is much greater. The net effect is that the electron trajectories are controlled by both the magnetic and electric fields, while the ion motion is affected only by the electric field, and the resulting motions can be uncoupled. From this, it follows that the predominant electron motion is the azimuthal **E**x**B** drift, since electrons are allowed to gyrate around B-field lines within the trap dimensions, and also gyrate around the discharge channel annulus, many times before undergoing a collision. In other words, the criteria in a Hall thruster discharge channel is such that the characteristic lengths and frequencies scale as follows: $r_{Li} >> r_{channel} >> r_{Le}$ and $\omega_{ce} > \Omega > \nu_{ne}$.

Classical cross-field electron mobility states that in a collisionless environment electrons would be indefinitely confined in azimuthal orbits. Collisions provide the only mechanism responsible for motion across B-field lines, through electron-neutral or electron-wall collisions, which allow an electron to "jump" to a new field line with a step length on the order of the Larmor radius. Therefore, increasing B slows cross-field diffusion by decreasing the Larmor radius and thus the step length. A detailed description of how this dependence comes about can be found in Chen[14].

Cross-field mobility is defined as the constant of proportionality between the cross-field velocity of electrons, u_{ez}, and the axial electric field, E_z:

$$\mu_{ez} \equiv \frac{u_{ez}}{E_z}. \tag{1}$$

An analysis of mobility is presented here based on the assumption of a large Hall parameter, that is $\omega_{ce}/\nu_{ne} >> 1$, a case that is required for Hall thruster operation. (In the situation that $\omega_{ce}/\nu_{ne} << 1$ magnetic field would have little effect on cross-field mobility, as electrons would have many collisions in a single gyration and would quickly eliminate the electric field necessary to produce thrust.) Given the case of a large Hall parameter, the cross-field electron velocity in radial magnetic and axial electric fields is given by classical model as:

$$u_{ez} = \frac{E_z}{B_r}\frac{\nu_{ne}}{\omega_{ce}}, \tag{2}$$

and thus mobility becomes

$$\mu_{ez} = \frac{\nu_{ne}}{B_r \omega_{ce}}. \tag{3}$$

Classical mobility can therefore be determined at any point in the discharge channel where the magnetic field is known and an effective collision frequency can be estimated accurately.

Although a number of methods for the experimental determination of cross-field mobility in Hall thrusters are well documented for a quasi-neutral plasma, certain considerations must be made when translating these concepts to a non-neutral plasma. Probably the most notable difference in these experiments is the existence of a space charge due to the absence of shielding ions. The existence of a negative space charge created by mutual repulsion of the electrons will induce a self-field that will locally depress the electric potential and drive the electrons to the walls of the trap; however, the magnitude of the space-charge field can be made negligible by adjusting the electron density.

The magnitude of the induced negative space charge is found from a solution of the Poisson equation $\nabla^2 \Phi = q n_e / \varepsilon_0$, where Φ is the electric potential. Since the experiments presented here are sensitive primarily to the radial space-charge field (the axial space-charge field is much less than the applied E-field and is a negligible perturbation), the experimental geometry is approximated as a cylindrical annulus infinite in the z-dimension with inner radius r_{in} and outer radius r_{out}. If the space between the cylinders is filled uniformly with electrons at density n_e=*constant*, then the solution to the Poisson equation for the space-charge potential relative to the local potential of the trap becomes

$$\frac{\Phi(r)}{n_e} = \frac{e}{4\varepsilon_0}\left[r_{out}^2 - r^2 + \left(r_{out}^2 - r_{in}^2\right)\frac{\ln\left(r_{out}/r\right)}{\ln\left(r_{in}/r_{out}\right)} \right]. \tag{4}$$

The maximum potential occurs midway between r_{in} and r_{out} where, for the physical scale of the apparatus used in the present investigation is, $\Phi_{max}/n_e \sim 1\text{x}10^{-11}$ Vm^3. Thus, if the electron density were limited to $n_e < 5\text{x}10^{10}$ m^{-3} (very typical for electron non-neutral particle traps[9]), then the space-charge potential at chamber mid-radius would be on the order of 1 V below unperturbed local trap potential. The moderate radial electric field induced by this 1 V

difference will not significantly alter the electron trajectories, as will be seen through an analysis of effective trap depth presented in Sec. II.b.).

Also significant is the application and control of an electric field in vacuum—rather than a self-consistent plasma—that could accurately reproduce conditions found in a Hall thruster. In a typical Hall thruster the impeded electron motion creates the electrostatic field necessary to accelerate propellant ions. Electric equipotential lines and magnetic field lines have been found to correspond in the quasi-neutral plasma[15] because electrons are mobile along field lines. The magnetic field and electric field are essentially orthogonal, giving rise to the dominant azimuthal electron motion and radial thermal motion. The approach used in this investigation reproduces the Hall thruster's defining fields with an externally-controlled electric field in vacuum in order to inspect a low-density pure electron plasma. In order to ensure that the E- and B-fields are orthogonal, the electrodes are curved to coincide with magnetic field lines. The result is aligned electric equipotential and magnetic field lines, and thus electrons are mobile along field lines.

III. Description of Methods

A. Electron Trapping Apparatus

An electron trapping apparatus shown in **Error! Reference source not found.** was constructed to reproduce the defining characteristics of a Hall thruster's accelerating region. The "confining volume," shown in Figure 1 is analogous to the discharge chamber in a Hall thruster. Electric and magnetic fields in the trap were designed using a numerical field solver (Maxwell®) and verified using a laboratory Hall sensor probe. Carefully shaped physical electrodes were employed to ensure that electric equipotentials coincided with magnetic field lines within the trap volume. The trap was designed with azimuthal symmetry in order to minimize variations in magnetic field over the annulus of the trap and to simplify electric and magnetic field models. Dimensions and field conditions were chosen for the trap such that the characteristic lengths and frequencies scale as follows: $r_{Li} >> r_{trap} >> r_{Le}$ and $\omega_{ce} > \Omega > \nu_{ne}$. The trap dimensions are on the order of 4 times larger than a typical 1.5 kW Hall thruster, with the outer diameter of the confining volume equal to 420 mm and a channel width of 100 mm. This allows us to operate in a wider range of B-field conditions, particularly low B-field, and still maintain scaling parameters. The magnetic field was produced by an inner and an outer coil inducing a field through iron magnet poles with the capability of producing a range of B-field magnitudes from ~30 Gauss to ~300 Gauss at the center of the confining volume. Much larger fields are possible with the present apparatus, however available power supplies limited testing to regions where B<300 Gauss for the present investigation. A representative magnetic field map for the region within the confining volume is shown in **Error! Reference source not found.**.

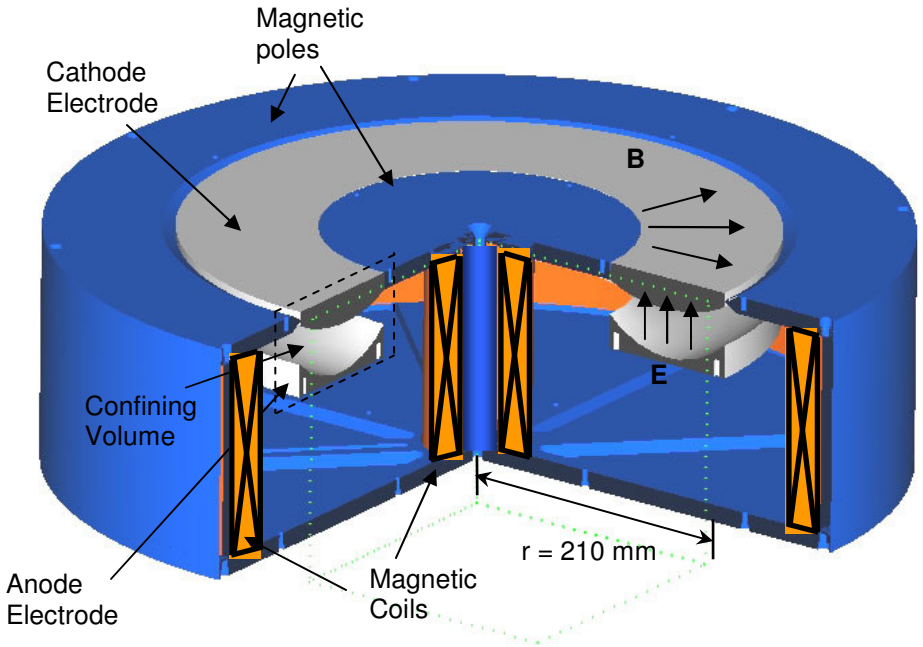

Figure 1. Electron trapping apparatus

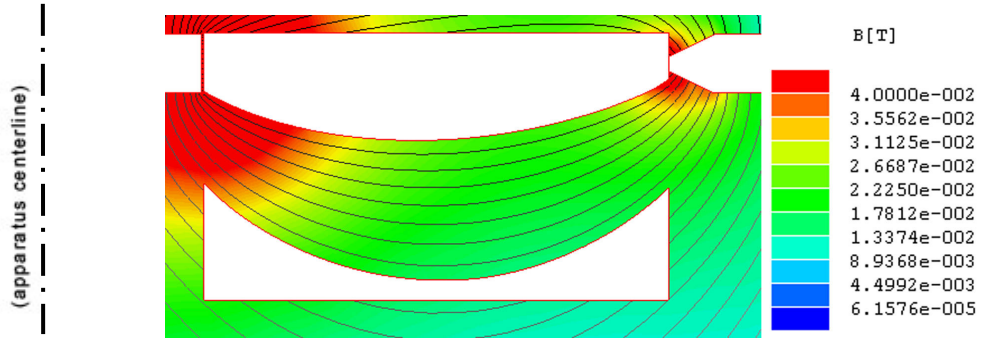

Figure 2. Contour plot of the magnetic field magnitude (field lines are superimposed).

The electric field in the region of interest was formed through electrodes in vacuum, rather than via a self-consistent plasma. The challenge in creating the electric field was meeting the criterion that magnetic field lines and lines of constant electric potential coincide. This was achieved through the use of curved electrodes whose surface contours were determined from magnetic field lines. In this design, electric equipotential lines are well aligned with magnetic field lines in a large percentage of the trap volume. A plot of electric potential is shown in Figure 3.

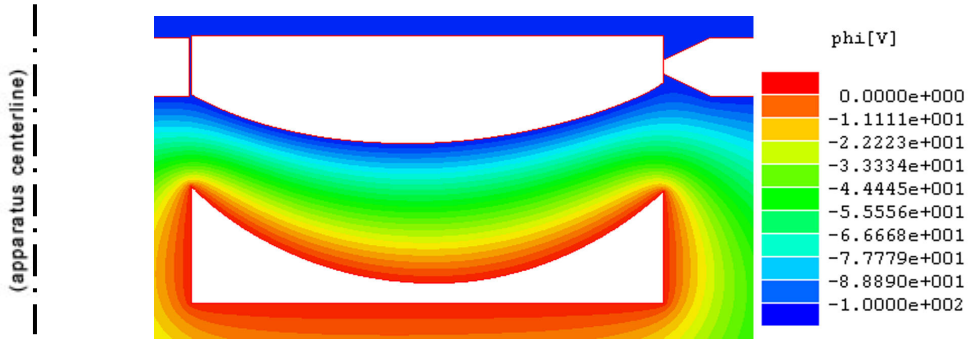

Figure 3. Contour plot of the trap electric potential

The B-field and electric equipotential lines from the contour plots are superimposed in Figure 4. Upon closer inspection it can be seen that the field lines, in fact, do coincide over a large fraction of the trapping width. This coincidence allows electrons to be thermally mobile along field lines within the trap, with the effective trap potential (described in more detail below) only varying by a few eV over the confining width, much like that of a Hall thruster. Equipotential lines depart from the magnetic field lines at the inner and outer radii of the trap creating a confining electric force at the trap edges, $\mathbf{F}_{E\|}$. This confining field emulates the plasma sheath found at dielectric walls of a Hall thruster discharge channel[4] and ensures radial confinement of electrons.

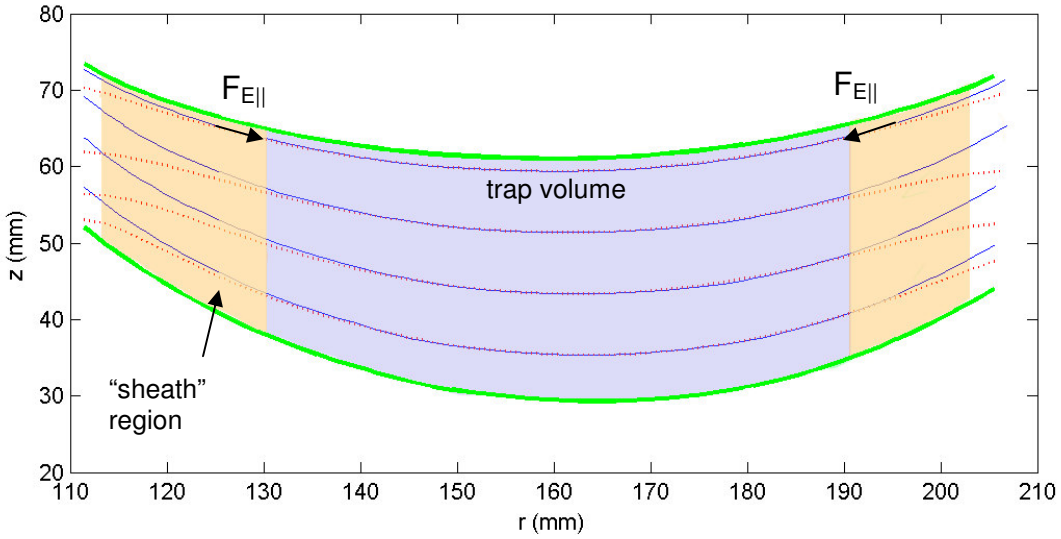

Figure 5. Cross sectional view of the confinement volume with magnetic field lines (solid) and electric equipotential lines (dashed) superimposed. Bold lines indicate electrode physical geometry.

The trap was loaded with electrons by passing a radial ~75 eV ionizing electron beam from a thermionic emitting filament through the trap from the outer pole. (i.e. The filament was biased 75 V below local potential. The absolute potential of the filament varied with E-field.) A schematic of this process is shown in Figure 5. While the high-energy beam electrons pass through and are collected on the inner pole surface, electron-ion pairs are created within the trap by collisions with background krypton neutrals. The energies of the secondary ejected electrons have been found to be on the order of 0.1 eV- 1eV for helium, neon and argon[16, 17] and similar ejected electron energies are expected for krypton. The unmagnetized krypton ions are immediately lost through collisions with the cathode, while the low-energy ejected electrons are trapped in azimuthal orbits via the applied fields. The filament emission current was monitored, so the filament heater circuit could be used as a control for electron density within the trap.

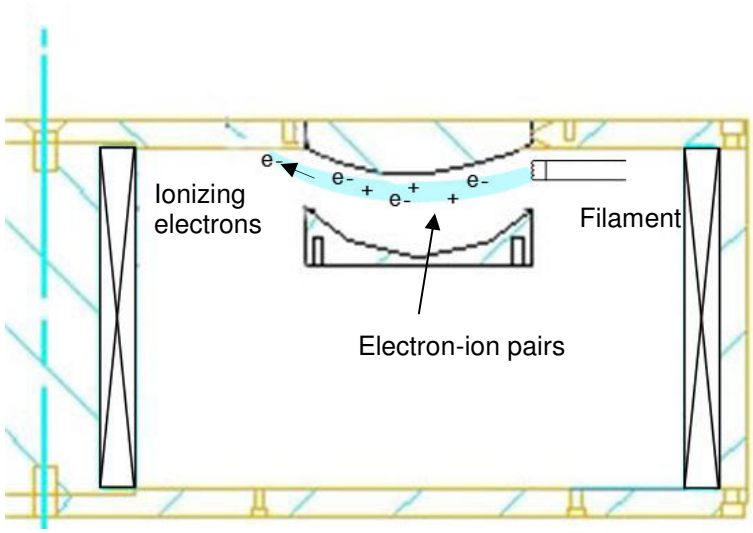

Figure 4. Trap loading schematic

B. Electron Motions Within Confinement Volume

The electron trap was designed in order to stably trap electrons with no dielectric walls—only with electric and magnetic fields. Stability was assessed by a two-dimensional analysis of the dominant forces acting on the electrons and integrating these to find an effective trap potential. All of these forces were evaluated along a magnetic field line with components parallel and perpendicular to the field line. Stability is critical in the direction of the field lines

as electrons are mobile along field lines but are confined axially on field lines. Thus the analysis presented here inspects the parallel component of the forces.

The forces acting on an electron parallel to the magnetic field are the magnetic mirror force, F_μ, due to the B-field gradient the parallel electric field force, $F_{E\|}$, due to deviation between electric equipotentials and magnetic field lines at the trap edges, and the centripetal force, F_C, due to the azimuthal drift velocity of electrons. The magnetic mirror force is given by

$$F_\mu = -\mu \nabla \mathbf{B} \bullet \hat{b} . \tag{5}$$

where $\hat{b}$ is the unit vector in the direction of the magnetic field vector given by $\hat{b} = \frac{\mathbf{B}}{B}$ and μ is the magnetic moment given by:

$$\mu = \frac{m u_\perp^{\,2}}{2B} \equiv \mu_0 = const. \tag{6}$$

The parallel electric field force acting along the field line is simply

$$F_{E\|} = q(\mathbf{E} \bullet \hat{b}) . \tag{7}$$

Finally, the centripetal acceleration due to the azimuthal ExB drift is given by

$$F_C = \frac{m u_{e\theta}^{\,2} \hat{r}}{r} \bullet \hat{b} = \frac{m(E_z B_r - B_z E_r)^2 \hat{r}}{r B^4} \bullet \hat{b} . \tag{8}$$

Thus, the net force acting on an electron is given by: $F_{net} = F_{E\|} + F_\mu + F_C$. Since we know the electric and magnetic fields at every point in the region of interest, and can assume a value for $u_\perp$ for the determination of μ_0, these equations can be numerically integrated in order to find an effective trap potential, Φ_{eff}, along a field line of interest which is given by:

$$\Phi_{eff}(r) = \int F_{net} dr . \tag{9}$$

Figure 6. a.) shows three representative field lines (red, green and blue; electrode geometry is represented by black lines) in the confinement volume in the case where B_r~150 Gauss and E_z~4x10^3 Volts/meter. The magnetic moment was determined using an electron perpendicular energy of 0.25 electron volts (representative of ejected electron energies from ionization) and a B_r of 150 Gauss. The force equations presented above were analyzed numerically along each of the field lines and are plotted in Figure 6. b.-d.) with corresponding colors. The net force along each field line is shown in Figure 6. e.) and the effective trap potential is shown in Figure 6. f.). It is notable that the parallel electric field force is by far the dominant force near the edges of the confinement volume but the parallel electric field force and magnetic mirror force are comparable and relatively small near the center of the confinement region. The effective potential of the trap is flat in the majority of the confinement volume indicating that electrons experience mostly thermal motion within the trap and are only strongly reflected at the edges of the trap.

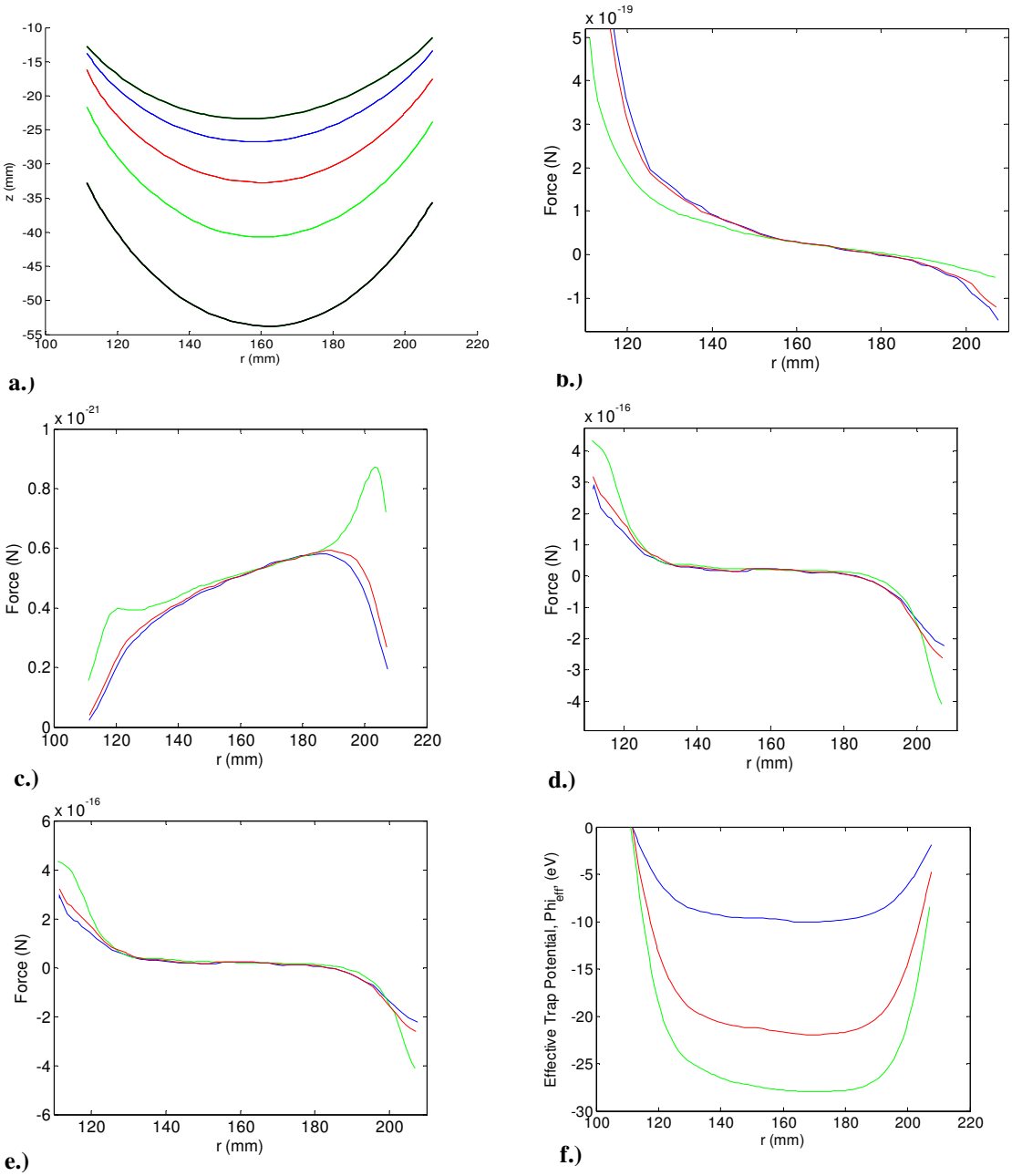

Figure 6. Dominant forces along representative field lines (arbitrary case): *a.) Three representative magnetic field lines, b.) Magnetic mirror force along each line, c.) Centrifugal force, d.) Parallel electric field force ,e.) Total forces, f.) Effective trap potential*

A confined electron has several characteristic frequencies within the trap. An electron undergoes a cyclotron motion as it gyrates around a field line, a magnetron motion as it traverses around the trap annulus due to the ExB drift, and a radial bounce frequency, which is described as the frequency at which an electron moves between the inner and outer walls of the trap. As previously described characteristic frequencies in the trap must scale as $\omega_{ce} > \Omega > \nu_{ne}$. Cyclotron frequency ($qB/m_e$) is typically on the order of 10^8-10^9 s^{-1} for the field conditions presented. Magnetron frequency, described as the number of cycles around the entire trap annulus per unit of time, is determined from $u_{e\theta}$ and an average trap radius ($\Omega = u_{e\theta}/2\pi r_{ave}$). Magnetron frequency is on the order of 10^5-10^6 s^{-1} scaling inversely with magnetic field. A bounce frequency is described as the frequency at which an electron moves

back and forth radially within the trap as it is reflected by the net confining forces at the trap edges. Electrons are created by the ionizing beam uniformly across the width of the confinement volume along a magnetic field line with very little perpendicular energy[16,17]. If an electron is born at the center of the trap potential it will only have thermal energy (0.1 – 1 eV) parallel to the field line and will have very little radial travel. However, if an electron is born near the edge of the trap it will gain radial energy from the effective trap potential as it "rolls" toward the center of the trap volume and will continue to "bounce" between the inner and outer radii of the trap.

Bounce frequency was determined numerically from the total time found for the electron to cross the channel width. For typical field conditions the bounce frequency was found to be on the order of 10^7 s^{-1} and did not vary greatly with varied field conditions. This frequency was also found to vary only minimally with the electron's radial starting position, indicating that this motion can be approximated by a simple harmonic oscillator. The bounce frequency falls below electron cyclotron frequency but above magnetron frequency, which indicates a radial bounce as the electron traverses azimuthally. This motion resembles the characteristic electron motion described by King[6].

Since mobility is governed by electron-neutral collisions and since the electron-neutral collision frequency scales with electron velocity, it is important to determine which component of electron motion dictates the collision frequency. The characteristic electron trap motions are used in determining an effective momentum transfer collision frequency, as collision frequency can vary greatly with electron temperatures below 5 electron volts[18]. Although in general the characteristic frequencies scale as $\omega_{ce} > \omega_B > \Omega$ within the operating regimes presented, the characteristic velocities corresponding to each of these frequencies ($u_\perp$, u_{eB} and $u_{e\theta}$, respectively) do not necessarily scale as simply. To determine an order of magnitude upper bound for collision frequency, we identify the highest electron velocity; thus we consider the condition where B is the lowest such that $u_{e\theta}$ is the greatest. At this point, the characteristic velocities scale as $u_{e\theta} > u_{eB} > u_\perp$. Based on an effective collision frequency model for krypton given by Baille[18], the effective collision frequency is on the order of 10^6 s^{-1} for operating pressures on the order of $5\text{x}10^{-6}$ torr. At the highest B fields investigated $u_{e\theta}$ drops by an order of magnitude which changes the scaling to $u_{eB} > u_{e\theta} > u_\perp$. In this case, had the effective collision frequency been determined based on $u_{e\theta}$, collision frequency would have been underestimated by more than three orders of magnitude. At large values of B the actual collision frequency is higher due to the bounce motion which then becomes the dominant motion of electrons. The effective velocity in this regime, u_{eB}, is orders of magnitude greater than the azimuthal velocity. The bounce motion then gives rise to a lower bound for collision frequency of $6\text{-}8\text{x}10^5$ s^{-1}.

C. Experimental Determination of Mobility

The cross-field mobility was evaluated experimentally by combining a measurement of the azimuthal Hall current with the axial (anode) current. The transverse mobility, μ_{ez}, is related to the electron density, n_e, the axial current flux, J_{ez}, and the axial E-field, E_z, by $J_{ez}=qn_e\mu_{ez}E_z$. Thus, if the anode collects electron current, I_a, over an area A_a, the mobility can be expressed as

$$\mu_{ez} = \frac{J_a}{qn_e E_z}. \tag{10}$$

Because we know the axial field at every point in the thruster we only need to obtain a measure of electron density in order to experimentally quantify mobility; this is obtained by measuring the azimuthal Hall current with an in-situ probe. The current density incident on the probe is J_p, where $J_p = qn_e u_{e\theta}$, and thus electron density can be determined, since $u_{e\theta} = E_z/B_r$, where both E_z and B_r are known from applied field conditions.
Rearranged, this gives

$$n_e = \frac{J_p B_r}{qE_z}. \tag{11}$$

By substitution, equation (10) simply becomes a ratio of the current density at the anode to the current density measured by the probe scaling with $1/B_r$:

$$\mu_{ez} = \frac{J_a}{B_r J_p}. \tag{12}$$

This method has the benefit that the mobility is indicated by the current density ratio, rather than the absolute values of each current. This uncouples the effect of varying electron emission or pair production rate on the measured mobility. This experimentally determined mobility can then be compared quantitatively with the classical model using Eqn. 3. Also as described in the previous section, the probe measurement was used to monitor n_e in order to ensure experiments are conducted within the space charge limitation.

For this in-situ measurement, a 2.36-mm-diameter probe was positioned 180 degrees opposite the ionizing electron beam, such that the probe does not collect current due to the high energy primaries but collects only lower energy, secondary electrons confined within the trap. The probe was biased 3V above local potential of the trap to be slightly attracting. This produced a negligible perturbation of the electric field of the trap and ensured that the probe was not repelling electron current should there have been error in field models or probe positioning. The probe was encased in an alumina sheath where the exposed collection area of the probe was aligned orthogonally to the azimuthal Hall current, as to collect only the directed flow of electrons. For typical field configurations to be investigated with this trap, namely B_r~50-200 G and E_z~1x10^4 V/m, an electron cloud with density ~5x10^{10} m^{-3} would create a probe current on the order of tens of nano-Amps. During the course of experiments electron density was monitored and controlled to keep the electron density well below the space charge limit.

All testing was performed in the Ion Space Propulsion Lab (Isp Lab) at Michigan Technological University. The testing facility consists of a 2-m-diameter, 4-m-long cylindrical vacuum chamber. Rough pumping is accomplished through a two-stage mechanical pump, capable of 400cfm. High vacuum is achieved through the use of three turbomolecular pumps with a combined throughput of 6,000 liters per second providing a base pressure below 10^{-6} Torr. Krypton gas was introduced to vary the base pressure from 10^{-6} to 10^{-4} Torr.

IV. Results and Analysis

From Eqn. 12 it follows that experimental cross-field mobility can be found solely by a current density ratio between the anode and an in-situ probe measurement, since we know B_r from applied fields. Currents were measured at the anode and the probe using a picoammeter and a digital source meter, respectively, in order to inspect mobility with changes in B-field magnitude, E-field magnitude and pressure (or equivalently, number density).

The variation in cross-field mobility as a function of magnetic field was determined by monitoring the probe and anode current as the radial magnetic field was varied from 0.003 T to 0.018 T (30-180 Gauss) under constant facility vacuum pressure. The results are shown in Figure 7**Error! Reference source not found.** with a solid line representing classical mobility. Colors indicate several sweeps done with all conditions held constant, with the exception of slight variations between sweeps in base pressure due to time lapse between data acquisition. For low magnetic fields, experimental and classical mobility was found to agree with only slight departures at fields above 0.01 T (100 Gauss).

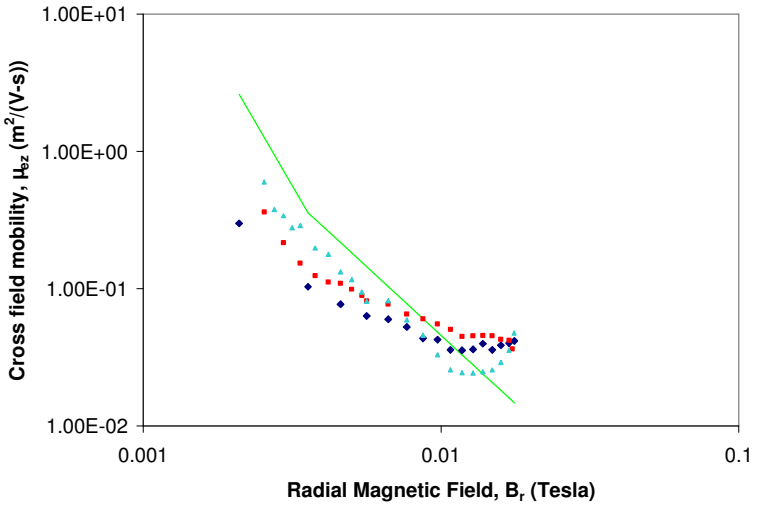

Figure 7. Cross-field mobility as it varies with radial magnetic field. Solid line represents classical mobility.

Classical mobility depends on collision frequency, cyclotron frequency, and radial magnetic field (Eqn. 3). The radial magnetic field and cyclotron frequency can be easily determined from applied fields. However, as described previously, determining an effective collision frequency is not entirely straightforward. Effective collision frequency was determined from a model presented by Baille et al[18] that gives collision frequency as a function of

electron temperature (or velocity) and number density since the momentum-transfer collision frequency has been found to vary greatly[18] with electron energies in the range of 0.1 to 5 eV. Therefore, a true representative electron velocity is needed in order to calculate an accurate collision frequency. Figure 8 shows characteristic electron velocities as they vary with B-field. Azimuthal velocity is simply $u_{e\theta} = E_z/B_r$ where both E_z and B_r are known from applied fields. Perpendicular velocity was calculated from the ejected electron energy (0.25 eV- 1eV corresponding to 2-4x10^4 m/s). Bounce velocity was determined numerically and was found to be on the order of 3-5 eV or 7-9x10^5 m/s.

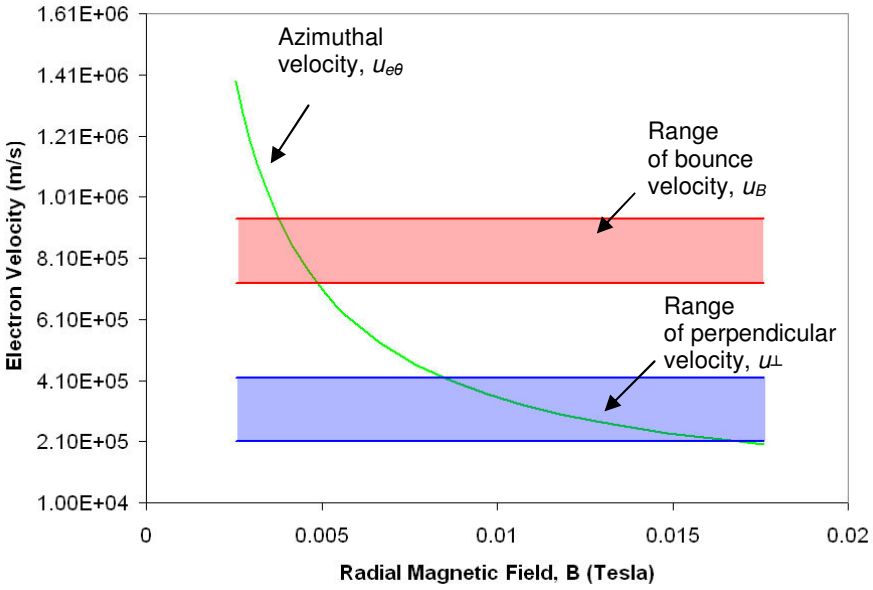

Figure 8. Analysis of electron velocity as it varies with B_r (constant E_z)

It is apparent that for low B-fields the azimuthal velocity is on the same order as the bounce velocity so either could be taken as the dominant electron motion; however, with increased B, the bounce velocity becomes the dominant motion as $u_{e\theta}$ drops by more than an order of magnitude. The motion can be described as an electron "rattling" back and forth radially through the trap as it slowly traverses azimuthally. Therefore in the general determination of collision frequency the true electron velocity must be selected as the maximum of bounce velocity and azimuthal velocity. Velocity perpendicular to the magnetic field, $u_\perp$, is taken as the electron thermal velocity and is well below both the bounce and azimuthal velocities. Using this method for determining collision frequency, classical mobility was plotted in Figure 7Figure . There is visibly a region where $u_{e\theta}$ is the dominant electron motion and a slight knee when the bounce velocity becomes the dominant electron motion. This method along with Baille's model was used in all subsequent theoretical determinations of cross-field mobility.

The variation of mobility with collision frequency was explored by bleeding background gas into the vacuum chamber. Krypton was introduced to the system to raise the base pressure from 9x10^{-7} to 1x10^{-4}, and the observed cross-field mobility is shown in Figure 9. Colors indicate sweeps taken at the magnetic field magnitudes shown. Classical mobility is shown as solid lines in corresponding color. Upon first inspection, the trends exhibited by the observed mobility are reasonable; mobility scales with increasing neutral density and decreases with increasing magnetic field. However, it is recognized that classical mobility scales linearly with neutral density, by realizing that collision frequency and neutral density are linearly related and $\mu_{ez} \propto \nu_{ne}$. Although the general trends of the observed mobility are understandable, the observed cross-field mobility was found to scale with $n_n^{1/2}$ through a power-law fit, rather than scaling linearly with n_n as would be expected by the classical model. An explanation for this odd departure is still absent, as the authors plan to investigate this more thoroughly in future experiments.

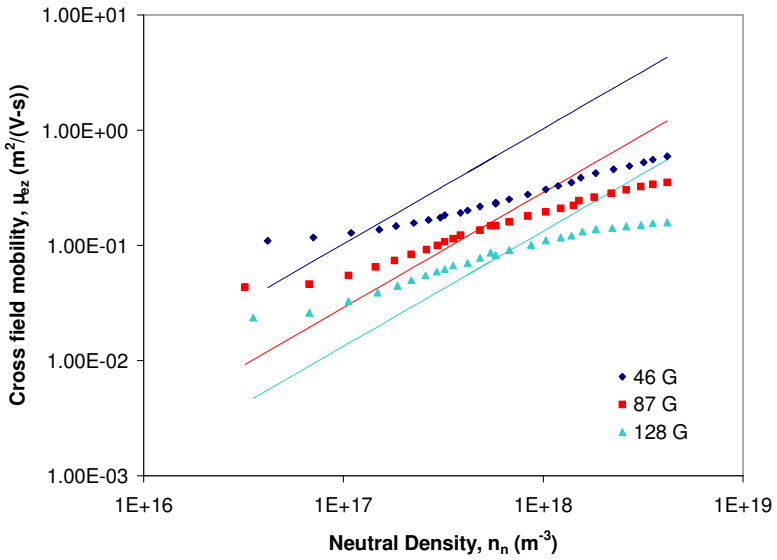

Figure 9. Cross-field mobility as it varies with neutral density for Kr. Solid lines in corresponding color indicate classical mobility

Cross-field mobility was observed with variations in electric field over an order of magnitude, from ~ $2x10^3$ to ~$1x10^4$ V/m and shown in Figure 10. Classical cross-field mobility is not expected to vary directly with electric field. However, an analysis of electron velocities in Figure 11 shows that in these field conditions the electron motion starts in a bounce dominated regime and then enters into a $u_{e\theta}$ dominated regime where, $u_{e\theta}$ scales linearly with E_z. Superimposing these two velocities gives the effective electron velocity over the electric field conditions considered. It follows, then, that collision frequency also varies over these field configurations translating to the non-constant classical mobility seen in Figure 10. Again there is good agreement between observed and classical mobility.

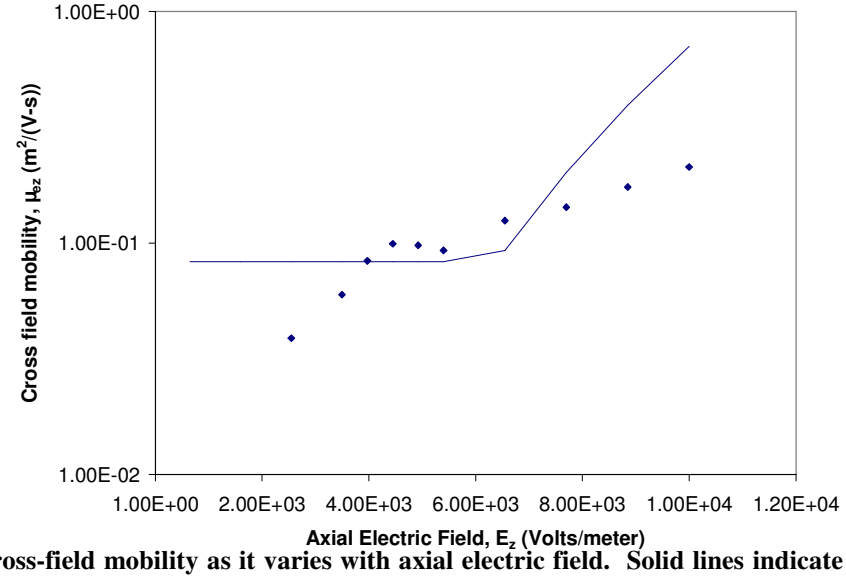

Figure 10. Cross-field mobility as it varies with axial electric field. Solid lines indicate an upper and lower bound for classical mobility

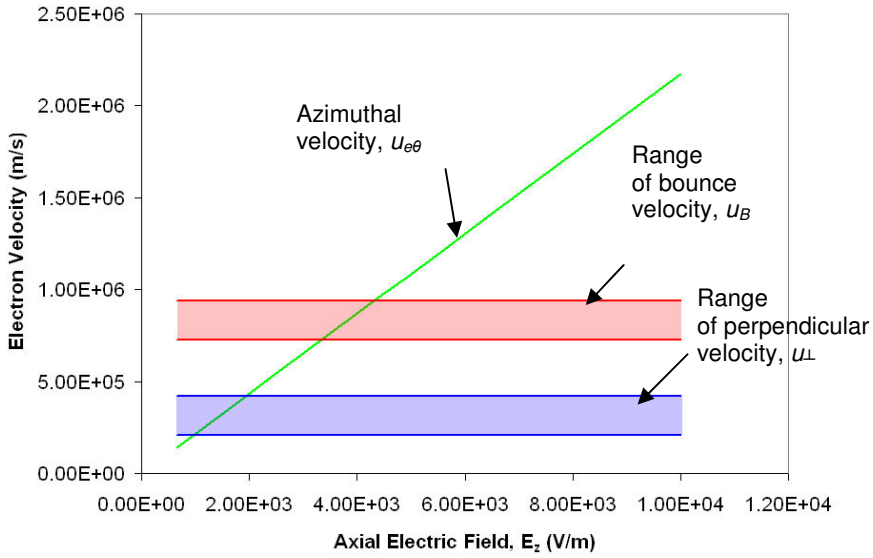

Figure 11. Analysis of electron velocity as it varies with E_z (constant B_r)

Over the conditions examined an electron density was observed to ensure all experiments were performed within the space charge limit. Figure 12 shows a plot of the electron number density as a function of B as measured by the electrostatic probe, with a maximum of 4.5×10^{10} m^{-3} which is well within our space charge limit.

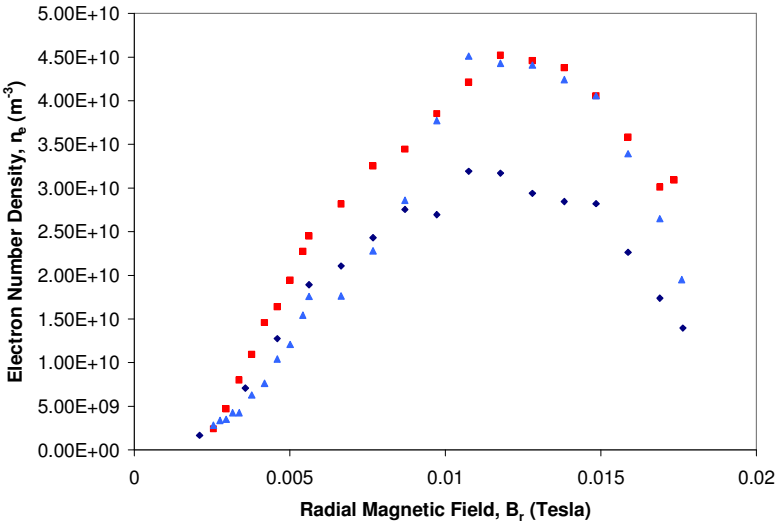

Figure 12. Electron number density as it varies with radial magnetic field.

The characteristic of the electron density profile as it varies with B is particularly interesting. At low B-fields, many high energy emitted electrons are lost because their Larmor radius is larger than trap dimensions. However, as B field is increased, more primary electrons are confined by the B-field and allowed to create electron-ion pairs. This trend is expected to increase to a saturation value where a maximum number of ionizing primaries are sent through the trap. However, instead of saturating, the electron density, as measured by the probe, sharply declined at fields above ~100 Gauss. This unusual characteristic is thought to be due to an artifact of the trap loading mechanism (see Figure 13**Error! Reference source not found.**). When the trap is loaded at low B-fields the Larmor radius of the primary ionizing electrons is on the order of the trap dimensions, creating electron-ion pairs

over the entire confinement volume of the trap. However, at high B-fields the primary ionizing electrons have a Larmor radius that is a fraction of the trap volume so electrons are only created in a small slice of the confinement volume, which is not seen directly by the probe. These two loading regimes have an obvious effect on the current incident at the probe, which could be mistaken as changes in mobility. In order to address this matter authors indend to incorporate an emitting filament that extends over the entire height of the confinement volume such that electrons are created uniformly over the confinement volume in all B-field conditions.

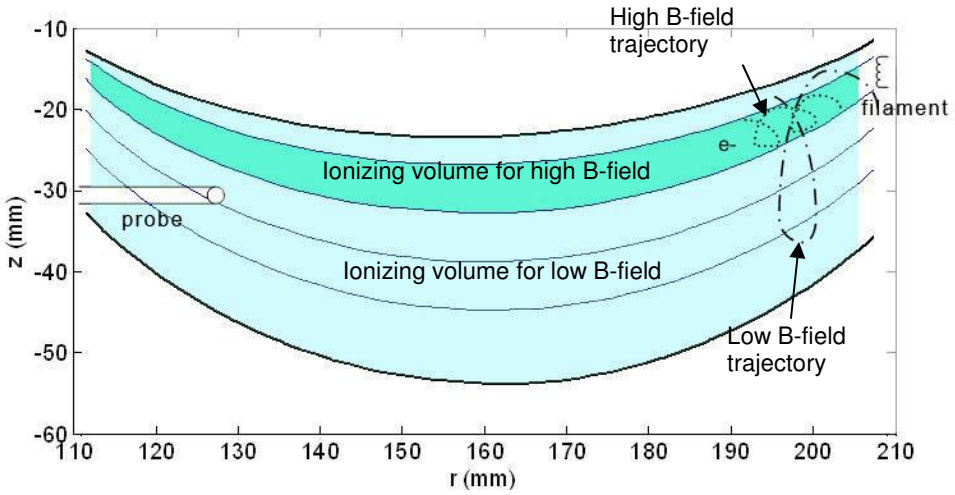

Figure 13. Schematic of trap loading mechanism.

V. Conclusions

Concepts have been explored for using a non-neutral plasma in order to study mobility in Hall thrusters. This paper presents a description of an apparatus that can be used to investigate electron mobility in Hall thruster fields absent from plasma effects and wall effects. The approach presented introduces a new method for Hall thruster research by decoupling the cross-field mobility from complicating plasma fluctuations and turbulence by conducting measurements on a pure electron plasma in a highly controlled environment. The first stage of this research was to measure mobility in simplified fields and to validate it against the classical mobility model. This method has been verified by the clear agreement between observed and classical cross-field mobilities with variations in magnetic and electric fields and neutral density. However, it was discovered from this research that an effective electron velocity is of utmost importance when calculating classical mobility. An accurate determination of classical mobility depends on an effective value of collision frequency, which can only be established through an analysis of dominant electron motions in the trap apparatus. The preliminary findings suggest that this method is suitable for Hall thruster research and will continue to be valid in more complex field environments. The ability to decouple electron motion from plasma effects and control the electric field externally gives rise to a wealth of experiments involving optimized magnetic fields or externally applied electrostatic perturbations.

Acknowledgments

The authors wish to acknowledge valuable discussions with and the assistance of Dean Massey and Alex Kieckhafer in this research. The authors would also like to acknowledge Master Machinist, Marty Toth, for all of the hard work and long hours required in the fabrication of the electron trapping apparatus. This work was supported by the National Science Foundation.

References

[1] Janes, G.S., and Lowder, R.S., "Anomalous Electron Diffusion and Ion Acceleration in a Low-Density Plasma," *Physics of Fluids*, **Vol. 9**, No. 6, (1966), pp. 1115-1123.

[2] Meezan, N.B., Hargus, W.A. Jr., and Cappelli, M.A., "Anomalous Electron Mobility in a Coaxial Hall Discharge Plasma," *Physical Review E.*, **Vol. 63**, No. 2, (2001) pp. 026410-1-7

[3] G. Guerrini and C. Michaut, "Characterization of high frequency oscillations in a small Hall-type thruster," *Physics of Plasmas,* **Vol. 6**, (1999) pp. 343.

[4] M. Keidar et al, "Plasma flow and plasma-wall transition in Hall Thruster Channel," *Physics of Plasmas*, **Vol. 8**, pp. 5315.

[5] J.P. Boeuf and L. Garrigues, "Low Frequency Oscillations in a Stationary Plasma Thruster," *Journal of Applied Physics*, **Vol. 84**, pp. 3541.

[6] King, L. B., "A (Re-)Examination of Electron Motion in Hall Thruster Fields", *29th International Electric Propulsion Conference*, IEPC-2005-258.

[7] Malmberg, J.H., Driscoll, C.F., Beck, B., Eggleston, D.L., Fajans, J., Fine, K., Huang, X.-P., and Hyatt, A.W., in Non-Neutral Plasma Physics, edited by C.W. Roberson and C.F. Driscoll, *AIP Conference Proc.* Vol. 175, No. 28, 1988.

[8] deGrassie, J.S., and Malmberg, J.H., "Waves and transport in the pure electron plasma," *Physics of Fluids*, **Vol. 23**, 63 (1980).

[9] Chao, E.H., Davidson, R.C., Paul, S.F., and Morrison, K.A., "Effects of background gas pressure on the dynamics of a nonneutral electron plasma confined in a Malmberg-Penning trap," *Physics of Plasmas*, **Vol. 7**, No. 3, March 2000, pp. 831-838.

[10] Robertson, S., and Walch, B., "Electron confinement in an annular Penning trap," *Physics of Plasmas*, **Vol. 7**, No. 6, June 2000, pp. 2340-2347.

[11] Espejo, J., Quraishi, Q., and Robertson, S., "Experimental measurement of neoclassic mobility in an annular Malmberg-Penning trap," *Physical Review Letters*, **Vol. 84**, No. 24, 12 June 2000, pp. 5520-5523.

[12] Robertson, S., Espejo, J., Kline, J., Quraishi, Q, Triplett, M., and Walch, B., "Neoclassical effects in the annular Penning trap," *Physics of Plasmas*, **Vol. 8**, No. 5, May 2001, pp. 1863-1869.

[13] for an extensive review of related non-neutral plasma trapping research see Bollinger, J.J., Spencer, R.L., and Davidson, R.C., eds., Non-neutral Plasma Physics, AIP Conference Proc. 498, Aug. 1999 and Dubin, D.H.E., and Schneider, D., eds., Trapped Charged Particles and Fundamental Physics, AIP Conference Proc. 457, Aug. 1998.

[14] Chen, F. F., *Introduction to Plasma Physics and Controlled Fusion*, 2nd ed., Plenum Press, New York, 1984, Chap. 5.

[15] Linnell, J. A. and Gallimore, A. D., "Internal Plasma Structure Measurements Using Xenon and Krypton Propellant," *International Electric Propulsion Conference*, IEPC2005-024.

[16] Peterson, W. K., Beaty, E. C., and Opal, C. B., "Measurements of Energy and Angular Distributions of Secondary Electrons Produced in Electron-Impact Ionization of Helium," *Physical Review A*, **Vol. 5**, No. 2, Feb. 1972, pp. 712-723

[17] Grissom, J. T., Compton, R. N. and Garrett, W. R., "Slow Electrons from Electron-Impact Ionization of He, Ne, and Ar," *Physical Review A*, **Vol. 6**, No. 3, Sept. 1972, pp. 977-987

[18] Baille, P., et al. "Effective Collision Frequency of Electrons in Noble Gases," *Journal of Physics B: Atomic and Molecular Physics*, **Vol. 14**, (1981), pp. 1485-1495.